New implementation to approximate quantum mechanical treatment of atom-diatom chemical reactions

ARTICLE *in* THE JOURNAL OF PHYSICAL CHEMISTRY · NOVEMBER 1986

Impact Factor: 2.78 · DOI: 10.1021/j100281a024

3 AUTHORS, INCLUDING:

Hiroki Nakamura
National Chiao Tung University
238 PUBLICATIONS **4,175** CITATIONS
SEE PROFILE

Michael Baer
Hebrew University of Jerusalem
345 PUBLICATIONS **8,235** CITATIONS
SEE PROFILE

New Implementation To Approximate Quantum Mechanical Treatment of Atom–Diatom Chemical Reactions

Hiroki Nakamura,* Akihiko Ohsaki, and Michael Baer†

Division of Theoretical Studies, Institute for Molecular Science, Myodaiji, Okazaki 444, Japan
(Received: May 5, 1986)

A new approximate quantum mechanical treatment of 3-D atom–diatom chemical reactions is proposed by combining the reactive infinite-order sudden approximation (RIOSA) and the collinear-type hyperspherical coordinate approach. Using the hyperspherical coordinate analysis of the potential energy surface and noticing the physical significance of the potential ridge, we can determine the matching parameter of the RIOSA without ambiguity at each γ, defined as the angle between the diatomic molecular axis and the atom–diatom relative translational coordinate vector. This solves the "arbitrariness" problem associated with the matching line within the RIOSA. It is also shown that one can have a better understanding of the reaction mechanisms by calculating eigenvalues as a function of hyperradius for each γ. Some numerical examples are presented to demonstrate these features.

1. Introduction

There is no doubt about the importance of quantum mechanical studies of chemical reaction dynamics. In an attempt to have a better understanding of the reaction mechanisms, various approximate quantum mechanical theories have been devised. The significance of developing good approximate theories is more emphasized by the fact that an exact quantum mechanical calculation is hardly feasible for a 3-D atom–diatom chemical reaction process

$$A + BC \rightarrow AB + C \qquad (1\text{-}1)$$

One reliable approximation proposed is the reactive infinite-order sudden approximation (RIOSA).[1] The ordinary IOSA has been proved to be effective in studying nonreactive atom–molecule collision processes,[2] and it was recently extended for reactive collisions as well.[3] The method has been applied to various systems[3b,4,5] and was found to be reliable for estimating vibrational state-to-state reactive cross sections. However, the method has one deficiency that has to do with the determination of the matching line. The matching line serves as a border line that separates the entrance and the exit channels and along which the reagents and the products wavefunctions are smoothly matched. This line can be proven to be straight, going through the origin, and therefore is determined by one single parameter—the matching parameter B. The value of B can be shown to be 1 for symmetric systems like $H + H_2 \rightarrow H_2 + H$ or $Cl + HCl \rightarrow ClH + Cl$. For all other cases B was estimated by employing qualitative arguments, but no sound method was available to yield a uniquely defined value for this parameter.

In this paper a method is proposed to determine B as a function of γ_i, which is the angle between the molecular axis of the diatomic BC and the relative translational coordinate vector of atom A with respect to BC (see Figure 1). The method is based on the physical significance of the so-called potential ridge, which provides a border line between reagent arrangement and product arrangement. It is essential for the determination of the position of potential ridge to employ the hyperspherical coordinates. Since within the RIOSA the 3-D configurations are projected onto collinear-type configurations, it is proposed that the collinear-type hyperspherical coordinates be employed, which are well-known to be effective for understanding the collinear reaction mechanisms.[6] The introduction of the hyperspherical coordinates in this context will enable an efficient numerical treatment of the RIOSA Schrödinger equation and will yield useful theoretical tools for analyzing the reactive system in its full dimensionality.

The organization of this paper is as follows: In section 2 the RIOSA is outlined briefly and is also analyzed to clarify its geometrical and physical implications. Section 3 is devoted to proposing a method for determining the matching parameter at each γ_i. Numerical examples are also given for the systems $He + H_2^+$ and $F + H_2$. A reformulation of the l-labeled RIOSA in terms of hyperspherical coordinates is given in section 4. Discussion is also given of how one can improve the understanding of the 3-D chemical reaction mechanisms by using collinear-type hyperspherical coordinates. The three systems, $He + H_2^+$, $F + H_2$, and $F + HCl$ are taken as examples. Conclusions are given in section 5.

2. Reactive IOS Approximation

The reactive infinite-order sudden approximation (RIOSA)[1,3] is outlined briefly for the sake of completeness. Some basic equations are also derived in this section to clarify the geometrical and physical implications of the approximation.

A. Outline of the l-Labeled RIOSA. Although there are two versions (J-labeled and l-labeled) of the RIOSA,[1,3] we outline here only the l-labeled theory. This is not only because the latter is supposed to be better in general but also because our new implementation of the RIOSA developed in this paper conforms better to the l-labeled version.

† IMS Visiting Professor. Permanent address: Soreq Nuclear Research Center, Yavne, Israel.

(1) Jellinek, J.; Kouri, D. J. *Theory of Chemical Reaction Dynamics*; Baer, M., Ed.; CRC: Boca Raton, FL, 1985; Vol. II, Chapter 1.

(2) Kouri, D. J. *Atom–Molecule Collision Theory*; Bernstein, R. B. Ed.; Plenum: New York and London, 1979; Chapter 9.

(3) (a) Khare, V.; Kouri, D. J.; Baer, M. *J. Chem. Phys.* **1979**, *71*, 1188. (b) Bowman, J. M.; Lee, K. T. *J. Chem. Phys.* **1980**, *72*, 5071. (c) Barg, G. D.; Drolshagen, G. *Chem. Phys.* **1980**, *47*, 209.

(4) (a) Kouri, D. J.; Khare, V. J.; Baer, M. *J. Chem. Phys.* **1981**, *75*, 1181. (b) Baer, M.; Jellinek, J.; Kouri, D. J. *J. Chem. Phys.* **1983**, *78*, 2962. (c) Abu-Salbi, N.; Shoemaker, C. L.; Kouri, D. J.; Jellinek, J.; Baer, M. *J. Chem. Phys.* **1984**, *80*, 3210. (d) Abu-Salbi, N.; Kouri, D. J.; Shima, Y.; Baer, M. *J. Chem. Phys.* **1985**, *82*, 2650. (e) Abu-Salbi, N.; Kim, S.-H.; Kouri, D. J.; Baer, M. *Chem. Phys. Lett.* **1984**, *112*, 502. (f) Clary, D. C.; Drolshagen, G. *J. Chem. Phys.* **1982**, *76*, 5027. (g) Clary, D. C. *Chem. Phys.* **1983**, *81*, 379. (h) Pollak, E.; Baer, M.; Abu-Salbi, N.; Kouri, D. J. *Chem. Phys.* **1985**, *99*, 15.

(5) (a) Baer, M.; Suzuki, S.; Tanaka, K.; Koyano, I.; Nakamura, H.; Hermann, Z.; Kouri, D. J. *Phys. Rev.* **1986**, *34A*, 1748. (b) Baer, M.; Nakamura, H.; Kouri, D. J. *Int. J. Quantum Chem.* **1986**, Symp. 20.

(6) (a) Manz, J. *Comments At. Mol. Phys.* **1985**, *17*, 91. (b) Nakamura, H.; Ohsaki, A. *J. Chem. Phys.* **1985**, *83*, 1599. (c) Bondi, D. K.; Connor, J. N. L.; Manz, J.; Römelt, J. *Mol. Phys.* **1983**, *50*, 467. (d) Aquilanti, V.; Cavalli, S.; Grossi, G.; Lagana, A. *J. Mol. Struct.* **1983**, *93*, 319; **1984**, *107*, 95.

0022-3654/86/2090-6176$01.50/0

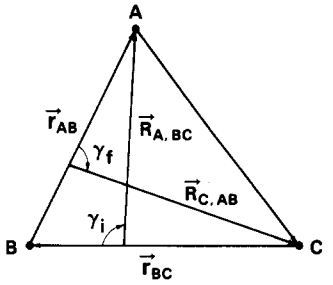

Figure 1. Coordinate vector diagram of the three-body system.

The basic Schrödinger equations to be solved in this approximation are (for simplicity we have taken $\vec{l} = \vec{l}_i$ and $\vec{j} = 0$, see eq 65 of ref 1)

$$\left\{-\frac{\hbar^2}{2\mu}\left(\frac{\partial^2}{\partial r_\lambda^2}+\frac{\partial^2}{\partial R_\lambda^2}\right)+\hbar^2\frac{l_\lambda(l_\lambda+1)}{2\mu R_\lambda^2}+ V(r_\lambda,R_\lambda:\gamma_\lambda)-E\right\} r_\lambda R_\lambda \Psi(r_\lambda,R_\lambda:\gamma_\lambda)=0; \qquad \lambda = \mathrm{i,\ f} \quad (2\text{-}1)$$

Here μ, r_λ, R_λ, and γ_λ are defined as

$$\mu = \left(\frac{m_A m_B m_C}{m_A+m_B+m_C}\right)^{1/2} \quad (2\text{-}2)$$

$$r_i = \left(\frac{\mu_{BC}}{\mu}\right)^{1/2} r_{BC} \qquad r_f = \left(\frac{\mu_{AB}}{\mu}\right)^{1/2} r_{AB} \quad (2\text{-}3)$$

$$R_i = \left(\frac{\mu_{A,BC}}{\mu}\right)^{1/2} R_{A,BC} \qquad R_f = \left(\frac{\mu_{C,AB}}{\mu}\right)^{1/2} R_{C,AB} \quad (2\text{-}4)$$

$$\gamma_i = \cos^{-1}(\hat{R}_{A,BC}\cdot\hat{r}_{BC}) \qquad \gamma_f = \cos^{-1}(\hat{R}_{C,AB}\cdot\hat{r}_{AB}) \quad (2\text{-}5)$$

where m_I is the mass of atom I, $\vec{r}_{IJ} = (r_{IJ},\hat{r}_{IJ})$ $[\vec{R}_{K,IJ} = (R_{K,IJ},\hat{R}_{K,IJ})]$ is the relative coordinate vector between I and J [K and IJ] (see Figure 1), and μ_{IJ} $[\mu_{K,IJ}]$ is the reduced mass of I and J [K and IJ] (I, J, K = A, B, C). The suffix i specifies the initial arrangement A + BC, and the suffix f designates the final arrangement AB + C of reaction 1-1. The quantities l_λ and $V(r_\lambda,R_\lambda:\gamma_\lambda)$ in eq 2-1 represent the angular momentum quantum number for the relative translational motion and the interaction potential energy at fixed γ_λ, respectively.

Solutions of the Schrödinger equations of the type (2-1) for the i- and f-arrangement channels are matched along a line, defined by

$$r_f = B_{fi} r_i \quad (2\text{-}6)$$

where B_{fi} is a γ_i-dependent constant. Equation 2-6 represents in general a conelike surface. However, it can be shown that for a fixed γ_i, this surface reduces to a straight line. For a given γ_i eq 2-6 also produces a single γ_f, given by

$$\cos\gamma_f = -\frac{\cos\gamma_i - (1-B_{fi}^2)\tan\alpha_i\cot\beta_{fi}}{B_{fi}(1+(1-B_{fi}^2)\tan^2\alpha_i)^{1/2}} \quad (2\text{-}7)$$

where

$$\tan\alpha_i \equiv [r_i/R_i \text{ on the matching line}] = \frac{\sin\beta_{fi}}{B_{fi}^2-\cos^2\beta_{fi}}\{-\cos\beta_{fi}\cos\gamma_i + (B_{fi}^2-\sin^2\gamma_i\cos^2\beta_{fi})^{1/2}\} \quad (2\text{-}8)$$

and β_{fi} is the skew angle defined by

$$\beta_{fi} = \tan^{-1}\left(\frac{m_B(m_A+m_B+m_C)}{m_A m_C}\right)^{1/2} \quad (2\text{-}9)$$

We can also derive

$$\tan\alpha_f \equiv [r_f/R_f \text{ on the matching line}] = \frac{B_{fi}}{(1+(1-B_{fi}^2)\tan^2\alpha_i)^{1/2}}\tan\alpha_i \quad (2\text{-}10)$$

Furthermore, since $r_i = (r_i^2+R_i^2)^{1/2}\sin\alpha_i$ and $r_f = (r_f^2+R_f^2)^{1/2}\sin\alpha_f = (r_i^2+R_i^2)^{1/2}\sin\alpha_f$ on the matching line, we have

$$B_{fi} = \sin\alpha_f/\sin\alpha_i \quad (2\text{-}11)$$

By matching solutions in the way mentioned above, we obtain a γ_i-dependent reactive scattering matrix element $S^{fp_f}_{il_ip_i}(\gamma_i)$, for the process $A + BC(v_i) \rightarrow AB + C(v_f)$, where the v's represent vibrational quantum numbers. From this S matrix we can calculate the ordinary full S matrix for state-to-state transition with specified rotational states.[1,3] Within the l-initial formulation the total cross section for the transition $v_i \rightarrow v_f$ is given as[1,7]

$$\sigma_{fi}(v_i\rightarrow v_f) = \frac{\pi}{2k_{v_i}^2}\sum_{l_i}(2l_i+1)\int_0^\pi |S^{fp_f}_{il_ip_i}(\gamma_i)|^2 \sin\gamma_i\, d\gamma_i \quad (2\text{-}12)$$

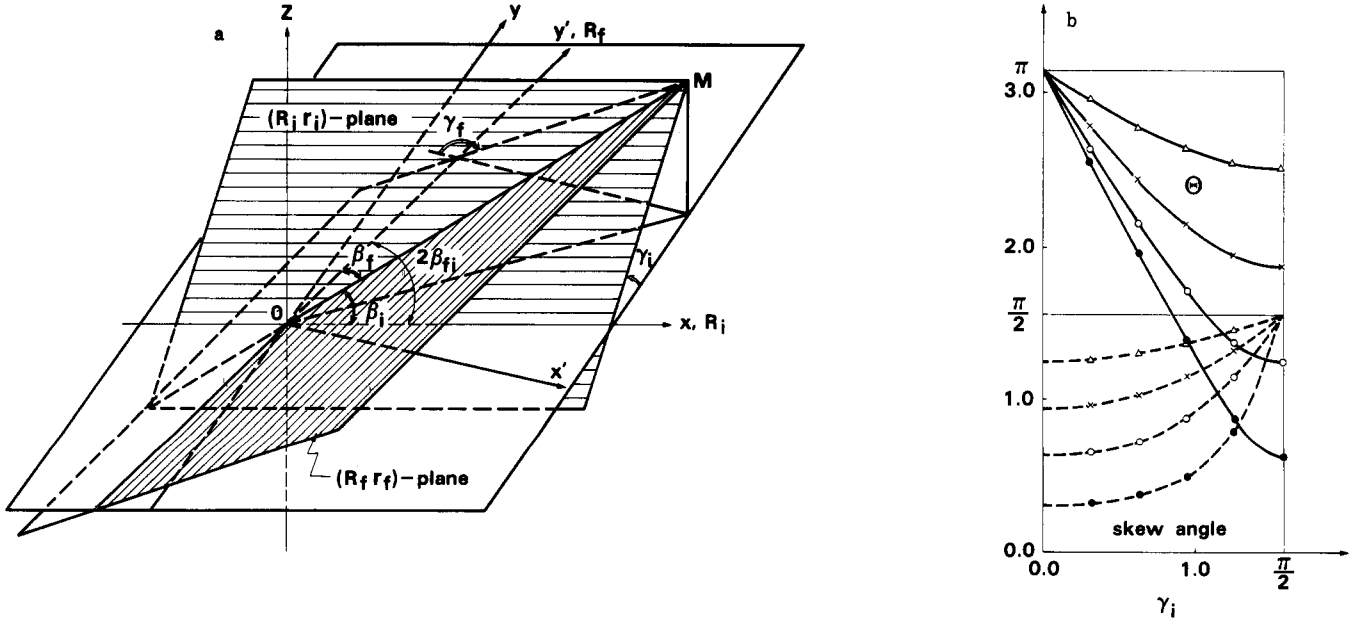

Figure 2. (a) Fixed γ initial (i) and final (f) arrangement channels. (R_i,r_i) and (R_f,r_f) are the fixed γ_i and fixed γ_f planes. The line OM is the matching line. (b) The γ_i dependence of Θ (solid lines) and $\beta_{fi}(\gamma_i)$ (dashed lines) for $B_{fi} = 1.0$. The skew angles at $\gamma_i = 0°$ $[\beta_{fi}(\gamma_i=0)]$ are $2\pi/5$, $3\pi/10$, $\pi/5$, and $\pi/10$ for △, ×, ○, and ●, respectively.

where k_{v_i} is the wavenumber in the initial channel.

B. Analyses of the Approximation. Since the angle γ is fixed in each arrangement channel, particles move on the plane defined by the two coordinates (R_i,r_i) or (R_f,r_f). The matching line is an intersection of these two planes. These features are depicted in Figure 2a. The x axis is taken along the coordinate R_i, and the x,y plane corresponds to a collinear arrangement ($\gamma_i = 0$). The skew angle is taken to be $2\beta_{fi}$ in order to have a symmetrical representation. In this coordinate system equations of the (R_i,r_i) and (R_f,r_f) planes are given respectively by

$$\frac{y}{\cos\gamma_i} - \frac{z}{\sin\gamma_i} = 0 \qquad (2\text{-}13a)$$

and

$$\frac{\sin 2\beta_{fi}}{\cos\gamma_f}x - \frac{\cos 2\beta_{fi}}{\cos\gamma_f}y + \frac{z}{\sin\gamma_f} = 0 \qquad (2\text{-}13b)$$

For the moment we treat γ_i and γ_f as independent variables, namely we do not apply the condition 2-6. The intersection line of the two planes is given by

$$\frac{x}{L} = \frac{y}{M} = \frac{z}{N} \qquad (2\text{-}14)$$

where

$$L = \frac{-\cos\gamma_i \sin\gamma_f \cos 2\beta_{fi} + \cos\gamma_f \sin\gamma_i}{\cos\gamma_f \cos\gamma_i \sin\gamma_f \sin\gamma_i} \qquad (2\text{-}15a)$$

$$M = -\frac{\sin 2\beta_{fi}}{\cos\gamma_f \sin\gamma_i} \qquad (2\text{-}15b)$$

and

$$N = -\frac{\sin 2\beta_{fi}}{\cos\gamma_f \cos\gamma_i} \qquad (2\text{-}15c)$$

The angle Θ between the two planes is obtained as

$$\cos\Theta = \cos\gamma_i \cos\gamma_f + \sin\gamma_i \sin\gamma_f \cos 2\beta_{fi} \qquad (2\text{-}16)$$

The angles β_i (and β_f) between the intersection line and the R_i (R_f) axis are given by

$$\tan\beta_i \equiv \tan\left[2\tan^{-1}\left(\frac{r_i}{R_i}\right)\right] = \frac{\sin 2\beta_{fi}}{\sin\gamma_i(\cot\gamma_i \cos 2\beta_{fi} - \cot\gamma_f)} \qquad (2\text{-}17a)$$

and

$$\tan\beta_f \equiv \tan\left[2\tan^{-1}\left(\frac{r_f}{R_f}\right)\right] = \frac{\sin 2\beta_{fi}}{\sin\gamma_f(\cot\gamma_i - \cot\gamma_f \cos 2\beta_{fi})} \qquad (2\text{-}17b)$$

Equations 2-17 are basically the same as those obtained by Grossi.[8]

The matching condition 2-6 makes γ_f and γ_i interrelated (cf. eq 2-7), and consequently Θ, β_i, and β_f become functions of γ_i, B_{fi}, and β_{fi}.

In the IOSA the two intersecting planes are flattened to make a single plane, namely the angle Θ is assumed to be π irrespective of the value of γ_i. The dynamics is then treated in the same way as in a collinear case. The only change is in the skew angle, which becomes

$$\beta_{fi}(\gamma_i) = \tfrac{1}{2}(\beta_f + \beta_i) = \alpha_f + \alpha_i \qquad (2\text{-}18)$$

For $\gamma_i = 0$, one can show that

$$\beta_{fi}(\gamma_i{=}0) = \beta_{fi} \quad \text{(given by eq 2-9)} \qquad (2\text{-}19)$$

as it should be. The flattening approximation is in general good for a heavy-atom transfer reaction, since in this case $\beta_{fi} \simeq \pi/2$, $\gamma_i + \gamma_f \simeq \pi$, and thus $\Theta \simeq \pi$ holds. In case of a light-atom transfer reaction we have $\Theta \simeq |\gamma_f - \gamma_i|$, and the flattening approximation is more crucial than in other cases. The validity of the approximation, however, depends also on the character of the dynamics. For instance, the approximation would not be so severe if the reaction process is strongly collinear dominated. As an example Θ and $\beta_{fi}(\gamma_i)$ for $B_{fi} = 1.0$ are shown in Figure 2b as a function of γ_i for various values of the collinear skew angles.

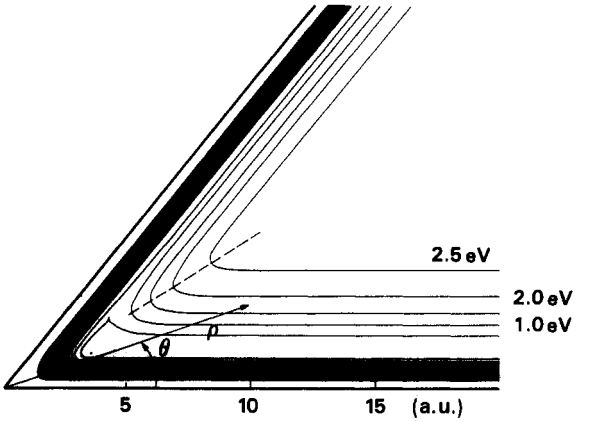

Figure 3. Equipotential contour plot of the HeH_2^+ collinear potential energy surface. The dashed line represents a ridge line. ρ and θ are hyperspherical coordinates.

3. Determination of the Matching Parameter

Although RIOSA was found to be quite useful for calculating reactive cross sections, it has, as mentioned before, one deficiency that has to do with the determination of the matching parameter B_{fi}. In this section we propose a method that obviates this defect and enables a rather unique determination of this parameter. This method gives, in general, a γ_i-dependent parameter. Some numerical examples are also presented to demonstrate how the method works.

A. Determination of γ-Dependent Matching Parameter. In a symmetric reaction such as $H + H_2 \rightarrow H_2 + H$, the matching parameter B_{fi} is 1. However, in a nonsymmetric case the value of B_{fi} is in general different from 1. In what follows a method is presented to determine its value. In order to do so we go back to the original physical meaning of the matching line and the IOS approximation. To start with we consider the collinear case. The matching line should, in principle, be a line that divides the whole coordinate space into two regions corresponding to the reagent arrangement channel and the product arrangement channel; in each of these the motion of the three atoms is described by the Schrödinger equation 2-1. In this sense the so-called potential ridge of the potential energy surface[6b] such as the one shown in Figure 3 is the best candidate to be a matching line. This can be more clearly understood if we draw potential energy curves such as those in Figure 4a using the hyperspherical coordinates ρ and θ, which are the polar coordinates, as is shown in Figure 3. Double-well potentials presented in Figure 4a are the cross sections of the potential energy surface at a fixed hyperradius ρ. The two wells in each curve represent a reagent channel valley and a product channel valley. The barrier in-between clearly separates the two valleys from each other. Therefore it is most reasonable to assume the ridge line to be the matching line. One problem is that a potential ridge is not necessarily a straight line, whereas according to the RIOSA this line has to be a straight line passing through the origin ($r = R = 0$). However, we found in all the cases studied so far that the ridge line is not far from a straight line and it is possible to determine the parameter B_{fi} without ambiguity. Once a value of the tangent, $\tan\alpha_i$, of the matching line is determined from the double-well potential energy curves, the matching parameter B_{fi} can be calculated from eq 2-11, since $\alpha_f = \beta_{fi} - \alpha_i$.

Next let us consider the noncollinear case. For each γ_i a constant parameter B_{fi} produces a single γ_f given by eq 2-7. The

(7) Kouri, D. J.; Khare, V.; Baer, M. *J. Chem. Phys.* **1981**, *75*, 1179.
(8) Grossi, G. *J. Chem. Phys.* **1984**, *81*, 3355.

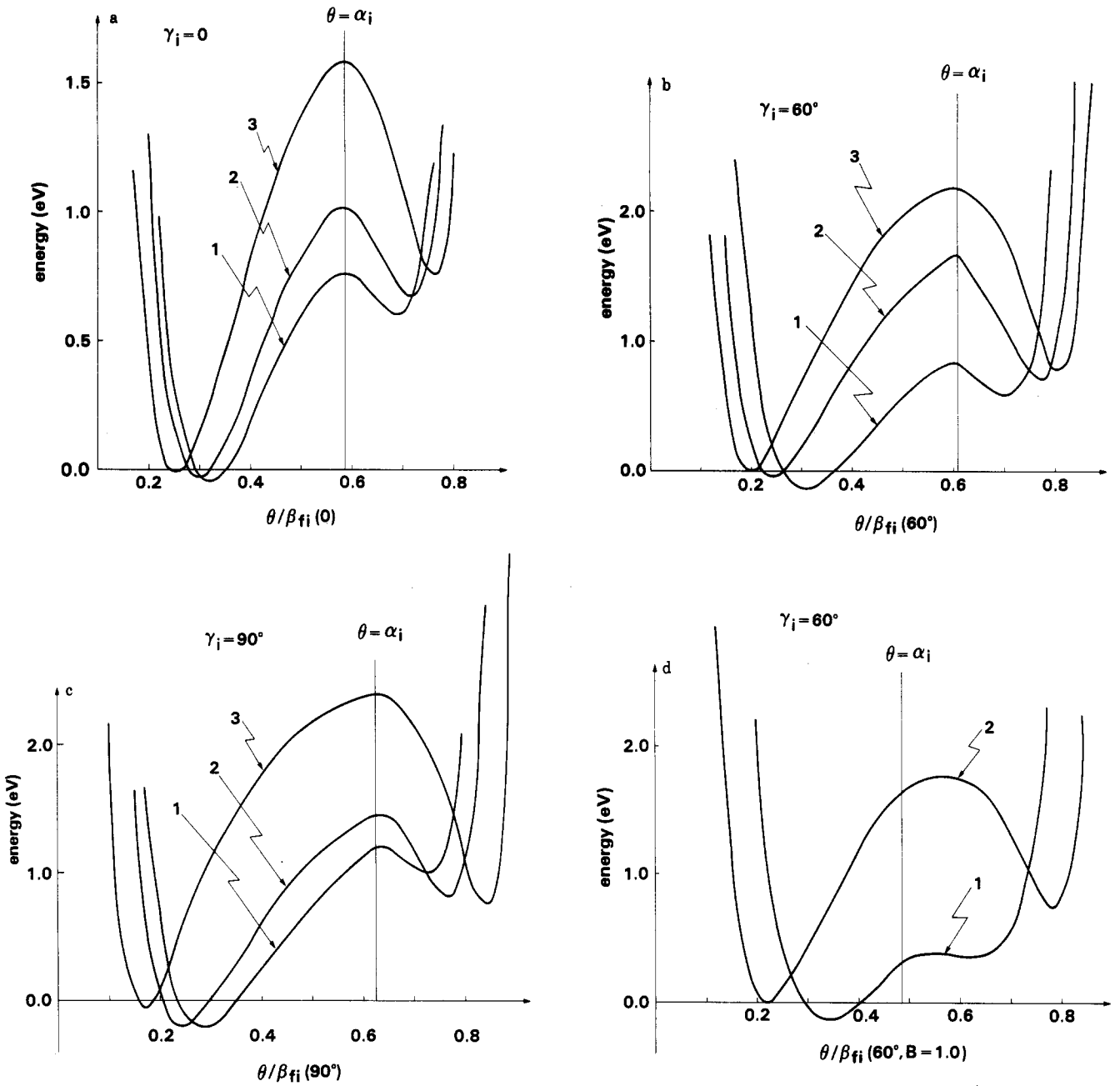

Figure 4. Double-minimum potential energy curves at fixed hyperradius ρ for HeH_2^+. (a) $\gamma_i = 0°$; 1, $\rho = 5.6a_0$; 2, $\rho = 6a_0$; 3, $\rho = 7a_0$. (b) $\gamma_i = 60°$; 1, $\rho = 4a_0$; 2, $\rho = 5a_0$; 3, $\rho = 6a_0$. (c) $\gamma_i = 90°$; 1, $\rho = 3a_0$; 2, $\rho = 4a_0$; 3, $\rho = 5a_0$. (d) $\gamma_i = 60°$; $B_{fi} = 1.0$; 1, $\rho = 4a_0$; 2, $\rho = 6a_0$.

dynamics in each arrangement channel is treated separately by solving the Schrödinger equation 2-1 from each asymptotic region to the matching line. The two wave functions thus obtained are matched along this line. Since γ_i and γ_f are fixed, the corresponding potential energy for the system can be represented in a two-dimensional space just like in the collinear case. Namely, the potential $W(r,R:\gamma_i)$ is given by

$$W(r,R:\gamma_i) = V(r_i,R_i:\gamma_i) \quad \text{for } 0 \le \theta \le \alpha_i(\gamma_i) \quad (3\text{-}1)$$
$$= V(r_f,R_f:\gamma_f) \quad \text{for } \alpha_i(\gamma_i) \le \theta \le \beta_{fi}(\gamma_i)$$

As in the collinear case we have, in general, a double-minimum potential as a function of θ at fixed ρ. Thus, it is again physically reasonable to identify the ridge line as the matching line. If an arbitrary value of B_{fi} is chosen, the tangent of matching line, tan α_i, can be calculated from eq 2-8 and the potential energy is given by eq 3-1. However, the position of the barrier in-between the two wells obtained from this potential does not necessarily yield a θ value that is equal to α_i. Thus the value of B_{fi} should be varied iteratively until the barrier position coincides with α_i. This iterative process is a kind of self-consistent procedure for determining the parameter B_{fi} at each given γ_i. The γ_i dependence of B_{fi} is considered to be natural, since the potential energy is dependent on γ_i. This dependence does not cause any difficulties in the RIOSA calculations, since the dynamics is solved separately at each γ_i and the total cross section is evaluated by integrating the reactive transition probability with respect to γ_i (see eq 2-12).

B. Numerical Examples. We have chosen the following two reactions:

$$He + H_2^+ \rightarrow HeH^+ + H \quad (3\text{-}2a)$$

and

$$F + H_2 \rightarrow FH + H \quad (3\text{-}2b)$$

as examples to demonstrate our method of determining B_{fi}.

The potential energy surface employed for the first reaction (3-2a) is the DIM potential of Whitton and Kuntz,[9] which was fitted to the ab initio calculations of Brown and Hayes.[10] Figure

(9) Whitton, W. N.; Kuntz, P. J. *J. Chem. Phys.* **1976**, *64*, 3624.
(10) Brown, P. J.; Hayes, E. F. *J. Chem. Phys.* **1971**, *55*, 922.

3 shows the potential energy contour for the collinear system. The dashed line represents a potential ridge. The position of the ridge can be more clearly manifested if we plot potential energies as a function of angle θ at fixed values of hyperradius ρ. Figure 4a shows such curves for the collinear case $\gamma_i = 0$. The left-side well corresponds to the reagent ($He + H_2^+$) valley and the right one to the product ($HeH^+ + H$) valley. The abscissa is the normalized angle θ/β_{fi}, where β_{fi} (=0.886 rad) is the skew angle defined by eq 2-9. The barrier position hardly varies with ρ, indicating that the ridge line is almost a straight line. From the barrier positions $\theta/\beta_{fi} = 0.59$, the parameter B_{fi} is calculated to be 0.7. Similar curves for $\gamma_i = 60°$ and 90° with $B_{fi} = 0.7$ are shown in Figure 4b,c. The ridge lines are almost straight lines. The abscissa is $\theta/\beta_{fi}(\gamma_i)$, where $\beta_{fi}(\gamma_i)$ is the angle defined by eq 2-18. The parameter B_{fi} is again found to be in both cases 0.7, indicating a weak dependence of B_{fi} on γ_i. This weak dependence is probably a reflection of the fact that the interaction potential of this system is rather isotropic.

Figure 4d demonstrates the fact that an improper choice ($B_{fi} = 1.0$) of the matching parameter produces an improper matching line. The vertical line is $\theta = \alpha_i$ ($\gamma_i = 60°$, $B_{fi} = 1.0$). This line does not go through the top of the barriers. If B_{fi} is changed, both the potential and α_i change. Thus the parameter B_{fi} should be determined in a self-consistent manner so that the maximum points of the barriers sit on the line $\theta = \alpha_i$.

Figure 5 shows similar diagrams for the reaction 3-2b. The potential energy surface employed is the Muckerman V.[11] The ridge line deviates slightly from a straight line, and the position of the barrier varies with ρ. However, this deviation is not significant at all and produces only a small percentage (less than 10%) of uncertainty in the values of B_{fi}. In the lower energy region we are interested in, B_{fi} is estimated to be 1.7 for $\gamma_i = 0°$ and 1.6 for $\gamma_i = 30°$ and 60°. The value used by Baer et al.[4b] is 1.4 for all γ_is, slightly smaller than the proper values.

4. Hyperspherical Coordinate Approach in the RIOS Approximation

In this section it is shown that the collinear-type hyperspherical coordinate approach can be employed within the framework of the IOSA and that by doing so the reaction mechanisms can be better visually understood.

A. Formulation in Terms of Hyperspherical Coordinates. As is easily conceivable from the discussions made in the previous two sections, the basic problem to be solved within RIOSA is essentially the same as that for the ordinary collinear reactions. Once the matching parameter B_{fi} is determined for a given γ_i, the potential energy surface by which the motion of three atoms is governed is given by eq 3-1 and is a function of two variables. Since the basic equations to be solved (eq 2-1) are the two-dimensional partial differential equations, the hyperspherical coordinates can be employed. The hyperspherical coordinate approach to collinear reactions has been successful not only in numerical procedures but also in the understanding of the reaction mechanisms.[6,12] Thus we think it is worthwhile to employ this method to study the 3-D chemical reactions within the IOSA.

In the ordinary RIOSA the two Schrödinger equations, eq 2-1 for $\lambda = i$ and f, are solved and the two solutions are matched along the matching line given by eq 2-6 for each fixed γ_i. Since the overall potential energy including a centrifugal potential should be continuous along the matching line, the relation

$$\frac{l_f(l_f + 1)}{R_f^2} = \frac{l_i(l_i + 1)}{R_i^2} \tag{4-1}$$

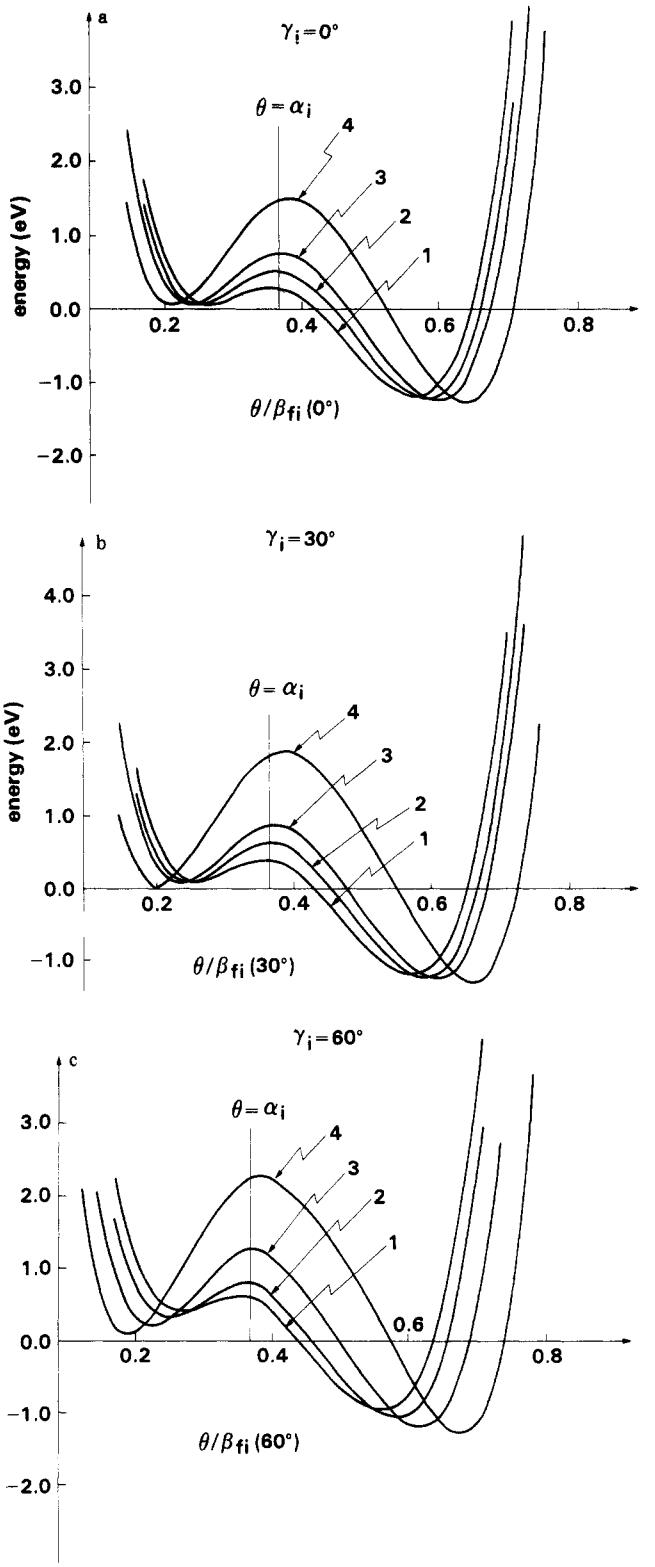

Figure 5. Double-minimum potential energy curves at a fixed hyperradius ρ for FH_2. (a) $\gamma_i = 0°$; 1, $\rho = 5a_0$; 2, $\rho = 5.2a_0$; 3, $\rho = 5.4a_0$; 4, $\rho = 6a_0$. (b) $\gamma_i = 30°$; 1, $\rho = 4.8a_0$; 2, $\rho = 5a_0$; 3, $\rho = 5.2a_0$; 4, $\rho = 6a_0$. (c) $\gamma_i = 60°$; 1, $\rho = 4a_0$, 2, $\rho = 4.2a_0$, 3, $\rho = 4.6a_0$, 4, $\rho = 5.4a_0$.

has to be satisfied on the matching line. Employing eq 2-6, 2-8, 2-10, and 2-11, one has

$$l_f(l_f + 1) = \left(B_{fi}\frac{\tan\alpha_i}{\tan\alpha_f}\right)^2 l_i(l_i + 1) = \left(\frac{\cos\alpha_f}{\cos\alpha_i}\right)^2 l_i(l_i + 1) \tag{4-2}$$

Since l_i is usually taken to be an integer, l_f cannot be, in general, an integer. The J-labeled IOSA[1,3] is not convenient, because the continuity condition can not be satisfied in this treatment.

(11) Muckerman, J. T. *Theoretical Chemistry: Advances and Perspectives*, Eyring, H., Henderson, E., Eds.; Academic: New York, 1981; Vol. 6, Part A.

(12) (a) Launay, J. M.; Le Dourneuf, M. *J. Phys. B* **1982**, *15*, L455. (b) Römelt, J. *Chem. Phys. Lett.* **1982**, *87*, 259.

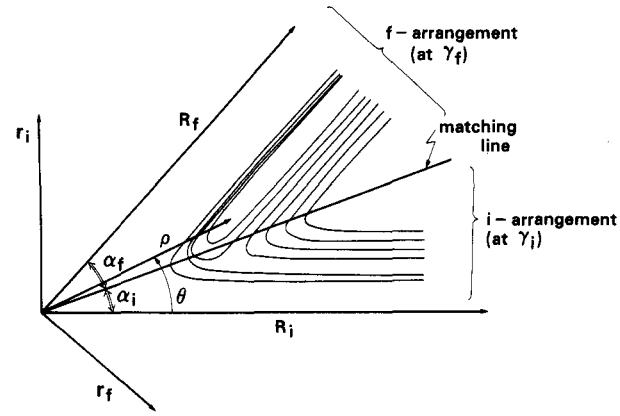

Figure 6. Schematic equipotential contour plot at fixed γ_i and γ_f and the corresponding hyperspherical coordinates.

Since the potential $W(r,R:\gamma_i)$ defined by eq 3-1 can be represented as in the ordinary collinear case, one can introduce hyperspherical coordinates ρ and θ as is shown in Figure 6. Thus for each γ_i one has to solve a single equation of the type

$$\left\{-\frac{\hbar^2}{2\mu}\left(\frac{\partial^2}{\partial\rho^2}+\frac{1}{\rho}\frac{\partial}{\partial\rho}+\frac{1}{\rho^2}\frac{\partial}{\partial\theta^2}\right)+W_{l_i}(\rho,\theta:\gamma_i)\right\}\Phi(\rho,\theta:\gamma_i)= E\Phi(\rho,\theta:\gamma_i) \quad (4\text{-}3)$$

where

$$W_{l_i}(\rho,\theta:\gamma_i) = W(r,R:\gamma_i)+\frac{\hbar^2 l_i(l_i+1)}{2\mu\rho^2\cos^2\theta} = V(r_i,R_i:\gamma_i)+\frac{\hbar^2 l_i(l_i+1)}{2\mu\rho^2\cos^2\theta} \quad \text{for } 0\le\theta\le\alpha_i \quad (4\text{-}4a)$$

$$W_{l_i}(\rho,\theta:\gamma_i) = W(r,R:\gamma_i)+\frac{\hbar^2 l_f(l_f+1)}{2\mu\rho^2\cos^2(\beta_{fi}(\gamma_i)-\theta)} = V(r_f,R_f:\gamma_f(\gamma_i))+\frac{\hbar^2 l_f(l_f+1)}{2\mu\rho^2\cos^2(\beta_{fi}(\gamma_i)-\theta)} \quad \text{for } \alpha_i\le\theta\le\beta_{fi}(\gamma_i) \quad (4\text{-}4b)$$

with $l_f(l_f+1)$ given by eq 4-2. The matching of two solutions required in the ordinary RIOSA is therefore not necessary here. The potential defined by eq 4-4 is not differentiable in the θ direction on the matching line, although it is almost smooth in that direction. This does not, however, cause any practical problems. As in the ordinary hyperspherical coordinate treatment of collinear reactions, the eigenvalue problem at each fixed ρ is solved first to give a set of potential energy curves $E_n(\rho)$ as a function of ρ, where n designates the nth eigenvalue corresponding asymptotically to a certain vibrational state of a diatomic (reagent or product) molecule. By looking into this diagram, $E_n(\rho)$ vs. ρ, one can understand some qualitative features of the dynamics of the reaction mechanisms. This point is discussed in the next subsection.

B. Better Understanding of Reaction Mechanisms. The hyperspherical coordinate approach is well-known to be a powerful tool for understanding the mechanisms of various collinear reactions. As was shown above, we can convey this power to a study of 3-D chemical reactions within the framework of the IOSA.

First, we take the same two examples (3-2a,-2b) as before. Figure 7 represents the eigenvalues of the HeH_2^+ system as a function of ρ at three values of γ_i (0°, 60°, 90°) for $l_i = 0$. The matching parameter B_{fi} was taken to be 0.7 as mentioned before. The dashed lines in these figures represent the potential ridges, where the nonadiabatic reactive vibrational transitions occur most effectively.[6b,6d,12a] From these figures one may obtain important features of this reaction. First, the potential energy curves are mostly strongly attractive except for $\gamma_i = 90°$. This indicates that the dynamics of this reaction system would be profoundly affected by many (Feshbach-type) resonances. This is already well-known from collinear quantum mechanical calculations.[13] Second, it

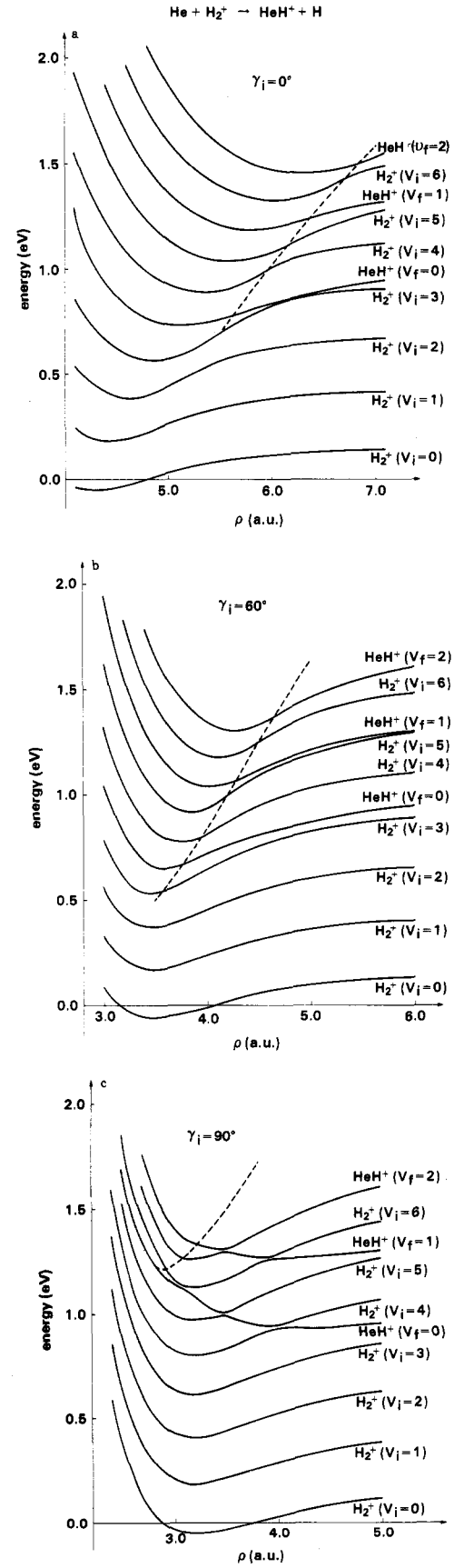

Figure 7. Adiabatic potential energies as a function of hyperradius ρ for the reaction He + $H_2^+(v_i)$ → $HeH^+(v_f)$ + H at a fixed value of γ_i: (a) $\gamma_i = 0°$; (b) $\gamma_i = 60°$; (c) $\gamma_i = 90°$.

is clearly seen that the energy stored in the vibrational mode is much more efficient in promoting the reaction than the translational energy. This is so because there are no reaction barriers,

(13) Kouri, D. J.; Baer, M. *Chem. Phys. Lett.* **1974**, *24*, 37.

as the attractiveness of the potential curves indicates, and because the reagent levels, asymptotically corresponding to lower vibrational states $v_i \leq 2$, lie far below the product levels at all ρ, and therefore the transitions to these states are less probable. This fact is also known not only from quasi-classical and quantum mechanical calculations but also from experiment.[5] Third, at large angles such as $\gamma_i = 90°$ (see Figure 7c) the reaction does not seem to be efficient at least for the states with initial vibrational levels $v_i = 0$–5, since the potential ridge lies in the small-ρ region and no effective avoided crossings exist there among the states corresponding to $v_i \leq 5$. Avoided crossings at larger ρ far from the ridge are sharp and probably do not have any dynamical significance. The calculations recently made with the ordinary RIOSA[5] actually indicate a sharp drop of cross sections at $\gamma_i \sim 90°$. Figure 8 shows some results of recent preliminary calculations (although these calculations were made with $B_{fi} = 0.8$ instead of 0.7, the results are not expected to differ significantly from the correct ones). Last, Figure 8 shows rather prominent peaks of $\sigma(\gamma_i;v_i)$ at $\gamma_i \simeq 50°$–$60°$ in the cases of $v_i = 4$ and 5. This could be explained by the potential energy curve diagram at $\gamma_i = 60°$ (Figure 7b). In comparison to the collinear case ($\gamma_i = 0$) (Figure 7a), the reagent levels, which asymptotically correspond to $v_i = 4$ and 5, lie much closer to the product levels around the ridge line. On the other hand, in the case of $v_i = 3$ the collinear configuration seems to be more favorable compared to the cases $v_i = 4$ and 5, since the reagent level of $v_i = 3$ lies closer to the product level of $v_f = 0$ than in the case of $\gamma_i = 60°$. Figure 8a actually shows that the peaks at $\gamma_i = 40°$–$60°$ are less profound. Potential energy diagrams for the second example (3-2b) are shown in Figure 9 for $\gamma_i = 0°$, 30°, and 60°. Exact hyperspherical coordinate treatment of the collinear reaction was made by Launay and Le Dourneuf and by Römelt.[12] Our potential energy diagram (Figure 9a) is slightly different from that of Launay and Le Dourneuf,[12a] since we assumed $\rho = 0$ to be the real origin ($r = R = 0$). It should be noted that the potential curves in Figure 9 are the adiabatic ones and that the fourth and fifth lowest curves have a very sharp avoided crossing at $\rho = 11$–$12a_0$.[12b] Since this avoided crossing is very sharp, it is practically correct to assume that these two levels have a real crossing there.[12b] Therefore the fourth [fifth] curve in Figure 9 practically correlates to HF(v_f=3) [$H_2(v_i$=0)] at $\rho = \infty$. Because of this level interchange the transition between $v_i = 0$ and $v_f = 2$ would probably become somewhat favorable. The potential curves for $v_i = 0$ and $v_f = 3$ are slightly more repulsive at $\gamma_i = 30°$ than at $\gamma_i = 0$. Thus the thresholds for the reactions $v_i = 0 \rightarrow v_f = 2$, 3 are expected to become slightly higher. At $\gamma_i = 60°$ all the potential curves are more repulsive and consequently the thresholds would become much higher. These features are qualitatively in accordance with the findings by Baer et al.[4b]

As a third example we have chosen the following light-atom transfer reaction:

$$F + HCl \rightarrow FH + Cl \qquad (4\text{-}5)$$

The potential employed is the LEPS of Ding et al.[14] The ridge line is almost a straight line, and the matching parameter B_{fi} is estimated to be 1.18 and is found to be hardly dependent on γ_i ($\leq 60°$). Calculated potential energies are shown in Figure 10 for $\gamma_i = 0°$, 30°, and 60°. The potential curves are mostly repulsive and thus the kinetic energy is important for the reaction to proceed. Furthermore, the ridge line moves rapidly to smaller ρ and higher energies with γ_i. This indicates that the reaction barrier gets higher and higher with increasing γ_i. Since the reaction is effective only at small γ_i, the flattening approximation described in section 2, which is in general rather severe for light-atom transfer reactions, is expected to be after all reasonable.

5. Concluding Remarks

Although the quantum mechanical RIOSA was found to be useful for estimating reactive cross sections of various kinds, there was one unsolved problem associated with determination of the matching parameter. In this paper we managed to solve this problem by employing the physical significance of potential ridge. It is not always possible to assign a theoretically unique value to

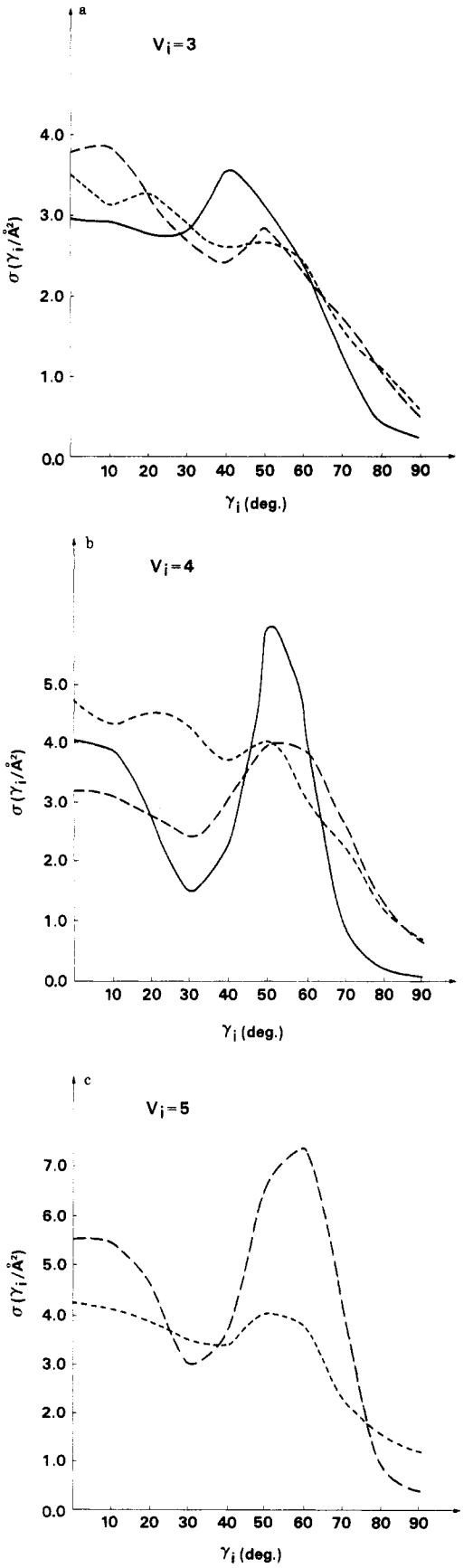

Figure 8. γ_i-Dependence of the reaction cross sections $\sigma(\gamma_i,v_i)$ for the reaction $He + H_2^+(v_i) \rightarrow HeH^+ + H$: (—) $E_{tot} = 1.3$ eV; (– – –) $E_{tot} = 1.5$ eV; (···) $E_{tot} = 1.8$ eV. (a) $v_i = 3$, (b) $v_i = 4$, (c) $v_i = 5$.

(14) Ding, A. M.; Kirsch, L. J.; Perry, D. S.; Polanyi, J. C.; Schreiber, J. L. *Faraday Discuss. Chem. Soc.* **1973**, *55*, 252.

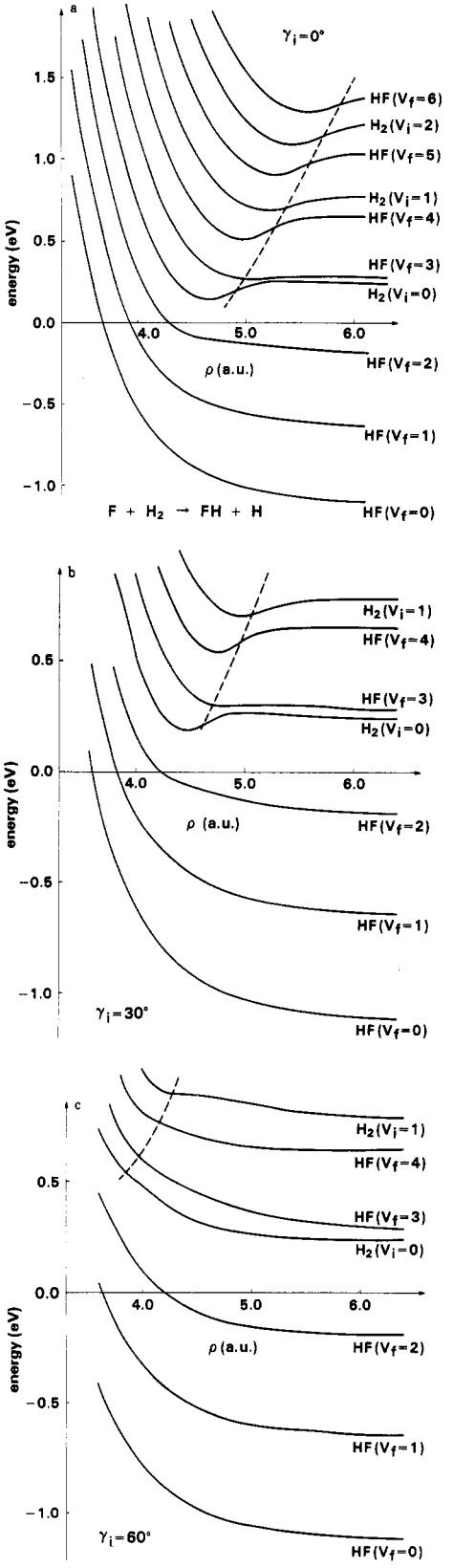

Figure 9. Adiabatic potential energies as a function of the hyperradius ρ for the reaction F + $H_2(v_i)$ → $FH(v_f)$ + H: (a) γ_i = 0°; (b) γ_i = 30°; (c) γ_i = 60°.

this parameter, because the potential ridge does not necessarily follow a straight line. However, in all cases studied so far there was no problem in assigning a reasonably well-defined value to this parameter. As a consequence the "arbitrariness" problem of the RIOSA is resolved.

It was also shown that dynamics calculations at each fixed γ_i can be carried out by using the collinear-type hyperspherical coordinates. An important point of doing this consists in the fact

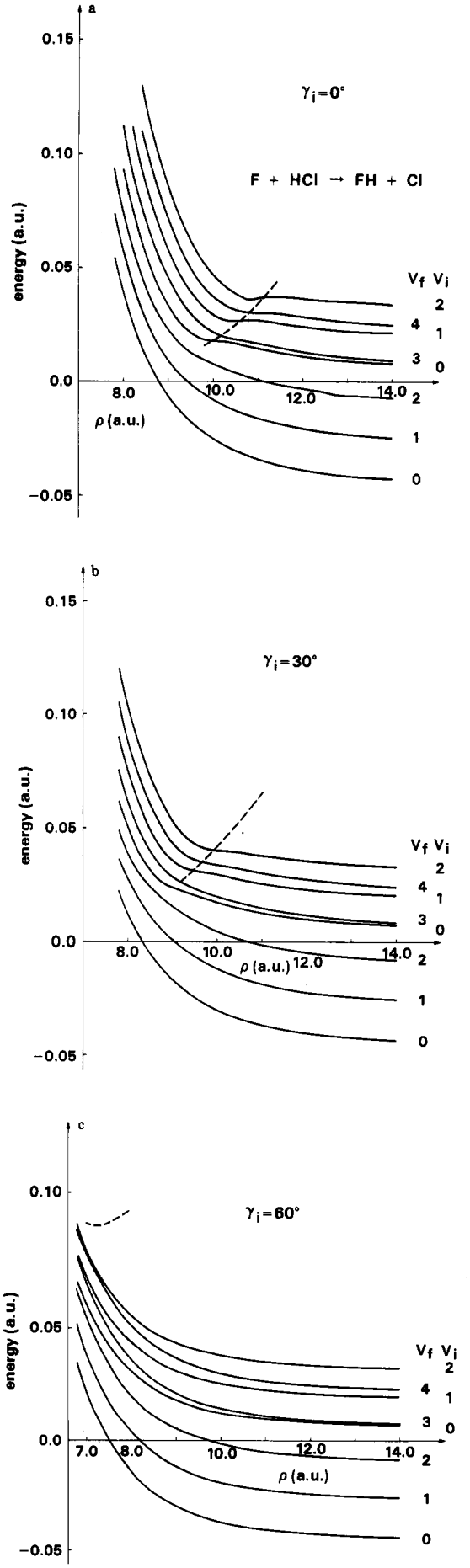

Figure 10. Adiabatic potential energies as a function of the hyperradius ρ for the reaction F + $HCl(v_i)$ → $FH(v_f)$ + Cl. (a) γ_i = 0°; (b) γ_i = 30°; (c) γ_i = 60°.

that the reaction mechanisms can be made more transparent. Namely, the power of the collinear hypershperical coordinates can be utilized straightforwardly in 3-D reactions. Some important qualitative features of the dynamics at each γ_i can be understood, for instance, by considering the potential energy diagrams, $E_n(\rho)$ vs. ρ, and the relative position of the γ_i-dependent potential ridge. Thus, the effects of the potential energy surface topography and the masses of the constituent atoms on the reaction dynamics can be conveniently investigated by the theory presented in this paper. In order to obtain values for differential and integral cross sections, one has to solve the Schrödinger equation. However, as a consequence of employing the hyperspherical coordinates, the numerical effort is reduced significantly just like in collinear reactions.

Acknowledgment. This work was supported in part by a Grant in Aid from the Ministry of Education, Science, and Culture of Japan. Numerical calculations were carried out at the computer center of the Institute for Molecular Science.

Photodissociation Studies of HNCO: Heat of Formation and Product Branching Ratios

Thomas A. Spiglanin,† Robert A. Perry, and David W. Chandler*

Combustion Research Facility, Sandia National Laboratories, Livermore, California 94550
(Received: June 2, 1986; In Final Form: July 29, 1986)

The heat of formation (ΔH_f(298 K)) of HNCO is determined to be $-24.9^{+0.7}_{-2.8}$ kcal/mol (based on ΔH_f(NH) = 85.2 kcal/mol). This value is obtained by measuring the threshold for the production of NH($a^1\Delta$) and by determining the energy contents of the NH fragment and the CO cofragment produced by photolysis of HNCO at wavelengths near the threshold. Saturated laser-induced fluorescence is used to determine the internal state distribution of NH($a^1\Delta$), and multiphoton ionization is used to measure the internal state distribution of CO. An upper limit for the branching ratio of NCO/NH production from photodissociation of HNCO at 193 nm is determined from an analysis of kinetic experiments to be 0.10. To clarify the mechanism of photodissociation, HNCO fluorescence-excitation and NH($a^1\Delta$) action spectra are also measured. They imply that two excited states of HNCO are present where only one had previously been considered.

I. Introduction

Nitrogen chemistry in flames has been studied in great detail over the past 25 years, but the chemistry of radicals such as NH and NCO in combustion is still a major area of investigation. The photolysis of isocyanic acid (HNCO) is a potential source of both NH and NCO radicals and has received a great deal of attention. Two important dissociation channels are[1-3]

$$\mathrm{HNCO} + h\nu \rightarrow \mathrm{NH}(a^1\Delta) + \mathrm{CO} \quad (1)$$

$$\rightarrow \mathrm{NCO} + \mathrm{H} \quad (2)$$

A study of the dissociation channels and the energetics of HNCO is of interest as isocyanic acid has been suggested as a potential intermediate in the conversion of fuel-bound nitrogen to oxides of nitrogen.[4-8]

Progress has been made toward a complete understanding of the mechanism of the photodissociation of HNCO. Dixon and Kirby measured and analyzed the absorption spectrum of HNCO from 2000 to 2820 Å. The low-energy portion of this spectrum revealed that the lowest excited singlet state of HNCO has an equilibrium geometry with an N–C–O bond angle of approximately 120°,[9] in contrast with the nearly linear N–C–O bond of the ground state.[10] Dixon and Kirby were not able to determine the absolute geometry of this excited state (cis or trans). Okabe investigated the excited states of HNCO with vacuum-UV light and found that excitation results in the production of several electronically excited species that subsequently fluoresce.[11]

Several recent dynamics studies have investigated reaction 1. This reaction leaves NH in an electronically excited state and is the lowest energy, spin-conserving process that directly produces NH + CO. Fujimoto, Umstead, and Lin measured the vibrational state distribution of the CO fragment produced by HNCO photolysis at 6.4 eV (193 nm).[3] The vibrational distribution roughly fits a statistical model that assumes all of the CO correlates with the production of NH in the $a^1\Delta$ state. The populations of the quantum states of NH($a^1\Delta$) that result from 6.4-eV photolysis of HNCO have been measured by Drozdoski, Baronavski, and McDonald.[2] They found the NH to be formed vibrationally cold (only $v = 0$ seen) and the rotational state distribution in $v = 0$ describable by a temperature of 1100 K. These investigators were not successful in an attempt to observe NCO by laser-induced fluorescence and concluded that the initial production of NCO by the 193-nm photolysis of HNCO is negligible. Nonetheless, excimer laser photolysis of HNCO is used to generate NCO radicals for kinetics experiments.[8] Although NCO can be produced in these experiments by a secondary reaction of NH($a^1\Delta$) with HNCO,[2] the issue of the photodissociation branching ratio [NCO]/[NH] is far from settled.

Although HNCO and NCO are thought to be important in combustion systems, there still exists disagreement concerning the thermochemistry of these compounds. As part of his photodissociation study of HNCO, Okabe measured the appearance threshold for NH($c^1\Pi$) and (based on a heat of formation of NH of 81 kcal/mol, a heat of formation of CO of −26.5 kcal/mol, and an electronic energy of NH($c^1\Pi$) of 43 645 cm^{-1} (124.8 kcal/mol)) calculated the heat of formation of HNCO to be −23 kcal/mol.[11] Recent measurements of the heat of formation of NH range from 84 to more than 90 kcal/mol.[12-19] Using ΔH_f(NH) = 85.2

† Sandia Postdoctoral Research Associate.

(1) Okabe, H. *Photochemistry of Small Molecules*; Wiley-Interscience: New York, 1978.
(2) Drozdoski, W. S.; Baronavski, A. P.; McDonald, J. R. *Chem. Phys. Lett.* **1979**, *64*, 421.
(3) Fujimoto, G. T.; Umstead, M. E.; Lin, M. C. *Chem. Phys.* **1982**, *65*, 197.
(4) Hayes, B. S.; Iverach, D.; Kirov, N. Y. *Symp. (Int.) Combust. [Proc.], 15th, 1974* **1975**, 1103.
(5) Fenimore, C. P. *Combust. Flame* **1976**, *26*, 249.
(6) Morley, C. *Combust. Flame* **1976**, *27*, 189.
(7) Haynes, B. S. *Combust. Flame* **1977**, *28*, 113.
(8) Perry, R. A. *J. Chem. Phys.* **1985**, *82*, 5485.
(9) Dixon, R. N.; Kirby, G. H. *Trans. Faraday Soc.* **1968**, *64*, 2002.
(10) Yamada, K. *J. Mol. Spectrosc.* **1980**, *79*, 323.
(11) Okabe, H. *J. Chem. Phys.* **1970**, *53*, 3507.
(12) Melius, C. F.; Binkley, J. S. Presented at the Meeting of the Western States Section of the Combustion Institute, University of California, Los Angeles, CA Oct. 17–18, 1983; paper WSS/CI 83-61.
(13) Melius, C. F.; Binkley, J. S. Presented at the 20th Symposium (International) on Combustion, The Combustion Institute, University of Michigan, Ann Arbor, MI, 1984.

0022-3654/86/2090-6184$01.50/0